Indian Journal of Chemical Technology
Vol. 30, January 2023, pp. 9-22
DOI: 10.56042/ijct.v30i1.68837

Entropy generation on chemically reactive hydromagnetic oscillating flow of third grade nanofluid in a porous channel with Cattaneo-Christov heat flux

A Subramanyam Reddy[1], K Govindarajulu*[,1], O Anwar Beg[2] & V Ramachandra Prasad[1]

[1]Department of Mathematics, Vellore Institute of Technology, Vellore-632 014, Tamil Nadu, India

[2]Multi-Physical Engineering Sciences Group, Mechanical Engineering Department, School of Science, Engineering and Environment (SEE), University of Salford, Manchester, M54WT, UK

E-mail: govind047@gmail.com

Received 18 November 2022; accepted 22 December 2022

The heat and mass transfer characteristics along with Cattaneo-Christov heat flux on oscillating hydromagnetic flow of third grade nanofluid through a permeable channel under entropy generation analysis have been examined in this paper. The impacts of chemical reaction, Brownian motion, thermophoresis, Ohmic heating, and radiative heat have also been taken into consideration. The Buongiorno nanofluid model has been utilized for the present analysis.The investigation related to the present study is helpful in biomedical engineering, manufacturing industries as coolants, energy conservation, cancer treatments (like hyperthermia), dynamics of physiological fluids, biomedicines, and nano-drug suspension in pharmaceuticals. The system of nonlinear ordinary differential equations (ODEs) have been attained and solved by applying the Runge-Kutta 4th order method with the help of shooting process after the execution of the perturbation procedure on non-dimensional partial differential equations (PDEs). The results of the present study have been deliberated by plotting graphs for the effects of various non-dimensional parameters on entropy, Bejan number, concentration, velocity, and temperature. The numerical values of heat and mass transfer rates for different physical parameters have been computed.

Keywords: Oscillating flow, Third grade nanofluid, Brownian motion, Thermophoresis, Entropy generation, Cattaneo-Christov heat flux

The pulsatile flow in a pipe/channel regarding inspections or studies have received much attention among the researchers and scientists due to its importance in the several fields like biomedical engineering, industries, and technological sciences. The composition of steady component and periodical time changing component (oscillating) is referred as pulsatile flow. As a special case, oscillating flow itself is a pulsatory flow when the steady component is zero. The concept of pulsatile flow has many applications such as respiratory systems, thermal insulation, urine flow in the ureter, the cooling of electronic components, circulatory systems, air conditioning, IC engines, vascular diseases, geothermal systems, reciprocating pumps, and blood dialysis process in an artificial kidneys[1–6]. Buren *et al.*[7] studied the heat transfer through pulsatory turbulent channel flow by using large eddy simulations. The finite element method is utilized in OpenFOAM to solve the flow governing equations. Zhang *et al.*[8] numerically and experimentally analysed the flow behaviour and enhancement of heat transfer of pulsating flow through a grooved channel by applying finite volume method. Kardgar[9] investigated the heat transfer and fluid flow in a rectangular cavity occupied with non-Newtonian nanofluid by using control volume finite volume method. Govindarajulu and Reddy[10] explored the effects of thermal radiation and Ohmic heating on pulsatory third grade hybrid nanoliquid flow in a penetrable channel with magnetic field and viscous dissipation impacts by applying bvp4c in MATLAB. Kot and Elmaboud[11] inspected the heat transfer phenomena on pulsating blood flow in a vertical stenosed artery under the effect of body acceleration by employing the Laplace and finite Hankel transformations. In this model, the fractional Cattaneo model is utilized and blood is taken as maxwell fluid.

Nowadays, research based on non-Newtonian fluids have attained much interest among researchers due to its wide range of applications in the fields of industries, science, and technology such as paper production, wiring coating, food processing, nourishment preparing, crystal growth, cosmetics,

coal slurries, clay mixture, oil recovery, rubber and plastic sheet drawing[12–14]. The fluids like paints, lubricants, blood at low shear rate, and oils are referred as non-Newtonian fluids because the shear stress and the rate of strain of these fluids show nonlinear relationship. Due to this, it is difficult to construct a single constitutive equation that has all properties to describe. Therefore, many researchers and scientists have modelled several non-Newtonian fluid models based on the rheological properties of non-Newtonian fluids. Amongst all the models, third grade fluid model is widely used and only model that describes both the shear thinning and shear thickening characteristics even in unidirectional and steady flows. The applications of Magnetohydrodynamics (MHD) play a vital role in many fields like drug industries, geology, astrophysics, and mechanical engineering, such as seismology, MHD generators, cosmology, and metallic sensors[15–17]. Considering these kinds of applications, many scientists and researchers investigated the importance of hydromagnetic flow in different flow geometries using various non-Newtonian fluid models [18,19]. In general, when the magnetic field is applied to the flow, the flow momentum will slow down which tends to influence some known effects such as Joule heating, Ion slip, and Hall current due to the strong applied magnetic field. These effects can influence the flow, mass and heat transfer characteristics in a non-negligible range. Amongst, the Joule heating effect is important while investigating MHD flows. Strengthening the magnetic field, some heat energy is generated due to the collision between the particles in a considerable range called as 'Joule heating or Ohmic heating'. The influence of Joule heating plays an important role in nuclear and geophysical engineering. The phenomena of Joule heating is important while investigating the MHD flow concerned studies because researchers and scientists are focussing on flows under the high magnetic field effect.

Nanofluids are fluids in which a nanosized particles (usually < 100nm) are deployed. The suspension of nanosized particles in the traditional base fluids like blood, water, and Ethelyn glycol shows an abnormal enhancement in heat transfer and thermal conductivity. Choi and Eastman[20] noticed this phenomenon while they inspecting the heat transfer characteristics of nanofluids. Nanofluids have numerous applications in heat transfer such as microelectronics, fuel cells and pharmaceutical industry, and in powered engines such as engine cooling, cancer treatment, vehicle thermal management, refrigerator, heat exchanger and boiler flue gas temperature reduction[21–24]. Recently, nanofluids are used in hyperthermia applications and chemotherapy. Buongiorno[25] inspected the thermophoresis and Brownian diffusions by introducing a new type of nanofluid model. Shah *et al.*[26] utilized the homotopy analysis technique to examine the third-grade nanoliquid flow via rotating parallel plates under the influence of Brownian motion and thermophoresis. Chu *et al.*[27] scrutinized the third-grade nanoliquid flow on an elastic surface with the impact of chemical reaction and activation energy by considering Buongiorno nanofluid model.

The analysis of entropy production is useful in fields like nuclear reactors, coolers, power plants, heat engines and pumps, air chillers, and solar energy systems. The energy which is unavailable to use as a mechanical energy in a system due to the random motion of molecules, spinning motion, and kinetic energy is called as entropy. The efficiency of the energy-oriented systems reduces because of the loss of heat energy. To overcome this, an optimization process is needed to reduce the irreversible energy as much as possible in the thermal systems. Bejan[28] was the first who constructed a mathematical relation on entropy generation and estimated the amount of heat energy that is unused. Later on, several researchers and scientists have done theoretical / experimental studies on entropy optimization and they suggested that it is possible to minimize the entropy production by selecting the suitable models/designs in efficient fluid systems[29–32].

The main purpose of several researchers and scientists is to develop a heat transfer system in which the transportation of heat enhances. The phenomena of heat transfer have vital role in the fields of biomedical engineering and manufacturing industries. For example, drug targeting, energy production, microelectronics, heat conduction in tissues, electronic devices cooling, fuel cells, cooling of nuclear reactor[33,34]. Fourier's heat conduction law characterizes the heat transfer features and having drawback that the parabolic energy equation is generated in this model, it is not applicable where the instant initial disturbances are also taken into account. To full out this kind of difficulty, Cattaneo[35] added the thermal relaxation time to Fourier's law and then Christov[36] modified the Cattaneo theory by adding the

thermal relaxation time derivative. Hayat *et al.*[37] investigated the Cattaneo-Christov theory on MHD stagnation dot non-Newtonian nanofluid flow towards an extendable sheet under the influence of thermophoretic and Brownian diffusions by applying optimal homotopy analysis method. Khan *et al.*[38] analytically inspected the mass and heat transfer using the theory of Cattaneo-Christov on non-Newtonian nanofluid flow via enlargeable sheet under magnetic field, Brownian and thermophoresis effects by utilizing the homotopy analysis approach. Ahmad *et al.*[39] scrutinized the stagnation point flow of non-Newtonian nanoliquid over an elastic non-linear surface under partial slip, buoyancy effect, and entropy with Cattaneo–Christov heat flux model by applying the finite difference scheme along with bvp4c from MATLAB.

As per the literature survey, no work has been made so far on basis of hydromagnetic oscillating flow of third-grade nanofluid through a permeable channel in the presence of Cattaneo-Christov heat flux model. To fill this research gap, we considered this concept for investigation by utilizing Buongiorno model. This type of research is noteworthy in biomedical engineering, manufacturing industries as coolants, energy conservation, cancer treatments like hyperthermia, dynamics of physiological fluids, biomedicines, and nano-drug suspension in pharmaceuticals. The main novelty of this study is analysing the hydromagnetic oscillatory flow of third-grade nanofluid in a porous channel with entropy generation and Cattaneo-Christov heat flux model. The impacts of Ohmic heating, thermal radiation, Brownian motion, thermophoretic diffusion, and chemical reaction are considered. The system of nonlinear ODEs are obtained and solved by applying the Runge-Kutta 4th order method with the help of shooting process after the execution of the perturbation procedure on non- dimensional PDEs. The impact of numerous pertinent physical parameters on flow variables are described graphically.

Formation of the problem

The pulsatile flow of third-grade nanofluid with Cattaneo-Christov heat flux between two horizontal permeable plates in the presence of applied magnetic field, thermophoresis, and Brownian motion is considered in this study. The flow is assumed aselectrically conducting laminar and incompressible. The impacts of Ohmic heating, viscous dissipation, radiative heat, and chemical reaction are taken into consideration. The flow geometry of the present model is presented in Fig. 1 that the x^*–axis is taken along with the direction of the lower wall, and the y^*–axis is taken as normal to the channel walls and h is the distance between the walls. A magnetic field of strength B_0 is uniformly applied orthogonal to the flow direction. v_0 is the fluid velocity which is injected through the bottom wall and with the same velocity rate it sucked out from the top wall. The top and bottom walls of the channel maintain the constant temperatures T_1, T_0 $(T_1 > T_0)$ and concentrations C_1, C_0 $(C_1 > C_0)$ respectively. With these concerned hypotheses, the flow governing equations are derived as:

$$\frac{\partial \mathrm{u}^*}{\partial \mathrm{t}^*} + v_0 \frac{\partial \mathrm{u}^*}{\partial y^*} = -\frac{1}{\rho_f}\frac{\partial P^*}{\partial x^*} + \frac{\mu_f}{\rho_f}\frac{\partial^2 u^*}{\partial y^{*2}} + \frac{\alpha_1}{\rho_f}\left(\frac{\partial^3 u^*}{\partial t^* \partial y^{*2}}\right) + 6\frac{\beta_3}{\rho_f}\left(\frac{\partial u^*}{\partial y^*}\right)^2\left(\frac{\partial^2 u^*}{\partial y^{*2}}\right) - \frac{\sigma_f}{\rho_f}B_0{}^2 u^* \quad \ldots (1)$$

$$\frac{\partial T^*}{\partial \mathrm{t}^*} + v_0 \frac{\partial T^*}{\partial y^*} + \lambda Q_E = \frac{k_f}{(\rho Cp)_f}\frac{\partial^2 T^*}{\partial y^{*2}} + \frac{\sigma_f}{(\rho Cp)_f}B_0{}^2 u^{*2} + \frac{\mu_f}{(\rho Cp)_f}\left(\frac{\partial u^*}{\partial y^*}\right)^2 + 2\frac{\beta_3}{(\rho Cp)_f}\left(\frac{\partial u^*}{\partial y^*}\right)^4$$

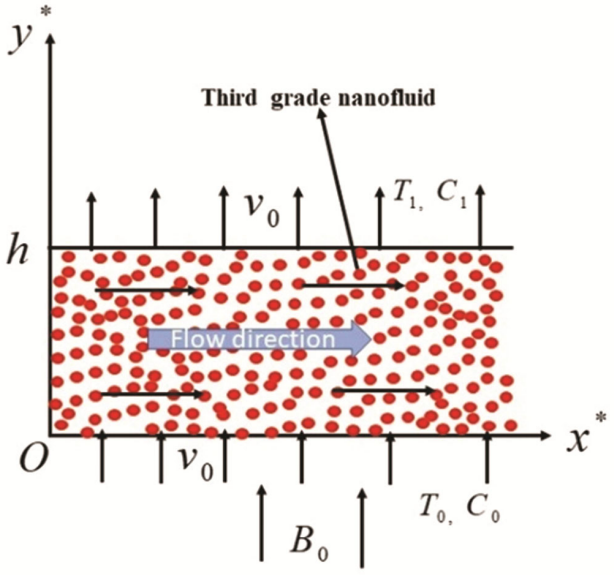

Fig. 1 — Physical model of the problem.

$$-\frac{1}{(\rho Cp)_f}\frac{\partial q_r}{\partial y^*}+\tau\left[D_B\frac{\partial C^*}{\partial y^*}\frac{\partial T^*}{\partial y^*}+\frac{D_T}{T_m}\left(\frac{\partial T^*}{\partial y^*}\right)^2\right], \quad \ldots (2)$$

$$\frac{\partial C^*}{\partial t^*}+v_0\frac{\partial C^*}{\partial y^*}=D_B\frac{\partial^2 C^*}{\partial y^{*2}}+\frac{D_T}{T_m}\frac{\partial^2 T^*}{\partial y^{*2}}-k_1C^*, \quad \ldots (3)$$

$$Q_E=\frac{\partial^2 T^*}{\partial t^{*2}}+2v_0\frac{\partial^2 T^*}{\partial t^*\partial y^*}+{v_0}^2\frac{\partial^2 T^*}{\partial y^{*2}}. \quad \ldots (4)$$

Here, u^* is the velocity component in the x^*- direction, P^* is the fluid pressure, ρ_f is density of the fluid, μ_f is the viscosity of fluid, α_1, β_3 are material constants, σ_f is electrical conductivity of the fluid, k_f is thermal conductivity, and $(\rho Cp)_f$ is effective specific heat of the fluid. T^* is the temperature, C^* is the concentration of nanoparticles, q_r is the radiative heat flux, $\tau=(\rho Cp)_p/(\rho Cp)_f$, $(\rho Cp)_p$ is the effective heat capacity of the nanoparticles, D_m and D_T are Brownian diffusion and thermophoretic diffusion coefficients respectively, T_m is mean temperature, and k_1 is the first order chemical reaction.

The appropriate boundary conditions (B.Cs) are:

at $y^*=0 \Rightarrow u^*=0,\ T^*=T_0,\ C^*=C_0,$ … (5)

at $y^*=h \Rightarrow u^*=0,\ T^*=T_1,\ C^*=C_1$ … (6)

With the utilization of the Rosseland approximation for radiative heat flux (q_r),Eq. (2) becomes

$$\frac{\partial T^*}{\partial t^*}+v_0\frac{\partial T^*}{\partial y^*}+\lambda Q_E=\frac{k_f}{(\rho Cp)_f}\frac{\partial^2 T^*}{\partial y^{*2}}+\frac{\sigma_f}{(\rho Cp)_f}B_0^2u^{*2}+\frac{\mu_f}{(\rho Cp)_f}\left(\frac{\partial u^*}{\partial y^*}\right)^2+2\frac{\beta_3}{(\rho Cp)_f}\left(\frac{\partial u^*}{\partial y^*}\right)^4$$

$$+\frac{1}{(\rho Cp)_f}\left(\frac{16\sigma^*}{3\kappa^*}T_1^3\right)\frac{\partial^2 T^*}{\partial y^{*2}}+\tau\left[D_B\frac{\partial C^*}{\partial y^*}\frac{\partial T^*}{\partial y^*}+\frac{D_T}{T_m}\left(\frac{\partial T^*}{\partial y^*}\right)^2\right], \quad \ldots (7)$$

here, κ^* is Rosseland mean absorption coefficient and σ^* is Stefan-Boltzmann constant.

Now, the dimensionless parameters and variables are chosen as,

$$u=\frac{u^*}{U},\ x=\frac{x^*}{h},\ y=\frac{y^*}{h},\ t=t^*\omega,\ P=\frac{hP^*}{\mu_f U},\ \theta=\frac{T^*-T_0}{T_1-T_0},\phi=\frac{C^*-C_0}{C_1-C_0}. \quad \ldots (8)$$

By utilizing Equ. (8),Eqs. (1), (3), and (7) are converted to

$$\frac{\partial u}{\partial t}+\frac{R}{H^2}\frac{\partial u}{\partial y}=-\frac{1}{H^2}\frac{\partial P}{\partial x}+\frac{1}{H^2}\frac{\partial^2 u}{\partial y^2}+\frac{1}{H^2}\gamma\frac{\partial^3 u}{\partial t\partial y^2}+\frac{6}{H^2}\Delta_1\left(\frac{\partial u}{\partial y}\right)^2\left(\frac{\partial^2 u}{\partial y^2}\right)-\frac{1}{H^2}M^2u, \quad \ldots (9)$$

$$\frac{\partial \theta}{\partial t}+\frac{R}{H^2}\frac{\partial \theta}{\partial y}+\Delta\left(\frac{\partial^2\theta}{\partial t^2}+2\frac{R}{H^2}\frac{\partial^2\theta}{\partial t\partial y}+\frac{R^2}{H^4}\frac{\partial^2\theta}{\partial y^2}\right)$$

$$=\left(1+\frac{4Rd}{3}\right)\frac{1}{H^2\,\mathrm{Pr}}\frac{\partial^2\theta}{\partial y^2}+\frac{Ec}{H^2}M^2u^2+\frac{Ec}{H^2}\left(\frac{\partial u}{\partial y}\right)^2$$

$$+2\frac{Ec}{H^2}\Delta_1\left(\frac{\partial u}{\partial y}\right)^4+\frac{Nb}{H^2}\frac{\partial\phi}{\partial y}\frac{\partial\theta}{\partial y}+\frac{Nt}{H^2}\left(\frac{\partial\theta}{\partial y}\right)^2, \quad \ldots (10)$$

$$\frac{\partial\phi}{\partial t}+\frac{R}{H^2}\frac{\partial\phi}{\partial y}=\frac{1}{H^2\,\mathrm{Pr}\,Le}\frac{\partial^2\phi}{\partial y^2}+\frac{1}{H^2\,\mathrm{Pr}\,Le}\frac{Nt}{Nb}\frac{\partial^2\theta}{\partial y^2}-\frac{\gamma_1}{H^2}\phi-\frac{K_1}{H^2}, \quad \ldots (11)$$

here, $H=\sqrt{\frac{\omega h^2}{\upsilon_f}}$ is frequency parameter, $\gamma=\frac{\alpha_1\omega}{\mu_f}$ is the material parameter for third-grade fluid, $\Delta_1=\frac{\beta_3U^2}{\mu_f h^2}$ is non-Newtonian coefficient, $\mathrm{Pr}=\frac{(\rho Cp)_f\upsilon_f}{k_f}$ is Prandtl number, $M=B_0h\sqrt{\frac{\sigma_f}{\mu_f}}$ is Hartmann number, $R=\frac{v_0h}{\upsilon_f}$ is cross flow Reynolds number, $\Delta=\lambda\omega$ thermal relaxation time parameter, $Rd=\frac{4\sigma^*T_1^3}{\kappa^*k_f}$ is the radiation parameter, $Ec=\frac{U^2}{(Cp)_f(T_1-T_0)}$ is the Eckert number, $Nb=\frac{\tau D_T(C_1-C_0)}{\upsilon_f}$ is Brownian motion parameter, $Nt=\frac{\tau D_B(T_1-T_0)}{T_m\upsilon_f}$ is thermophoresis parameter, $Le=\frac{k_f}{D_B(\rho Cp)_f}$ is Lewis number, $\gamma_1=\frac{k_1h^2}{\upsilon_f}$ is chemical reaction parameter, $K_1=\frac{k_1C_0h^2}{\upsilon_f(C_1-C_0)}$ is constant, U is characteristic velocity, ω is frequency.

The corresponding B.Cs are

at $y=0 \Rightarrow u=0,\ \theta=0,\ \phi=0,$ … (12)

at $y=1 \Rightarrow u=0,\ \theta=1,\ \phi=1.$ … (13)

Solution of the Problem

Since the flow is driven by the pressure gradient, the dimensionless pressure gradient is taken as:

$-\frac{\partial P}{\partial x}=\lambda_0+\varepsilon\lambda_1e^{it}$, where … (14)

On the basis of Eq. (14), the solutions for u , θ, and ϕ are expressed as

$$u = u_0 + \varepsilon u_1 e^{it}, \quad \ldots(15)$$

$$\theta = \theta_0 + \varepsilon \theta_1 e^{it}, \quad \ldots (16)$$

$$\phi = \phi_0 + \varepsilon \phi_1 e^{it}, \quad \ldots (17)$$

Now, taking the Eqs.(14)-(17) into Eqs (9) - (11) and by equating thecorresponding coefficients of different powers of ε , we can obtain the set of ordinary differential equations

$$\left(1 + 6\Delta_1 u_0'^2\right) u_0'' - R u_0' - M^2 u_0 + \lambda_0 = 0 \quad \ldots (18)$$

$$\left(1 + i\gamma + 6\Delta_1 u_0'^2\right) u_1'' - R u_1' + 12\Delta_1 u_0' u_0'' u_1' - \left(M^2 + iH^2\right) u_1 + \lambda_1 = 0, \quad \ldots (19)$$

$$\left[\left(1 + \frac{4Rd}{3}\right)\frac{1}{\Pr} - \frac{\Delta R^2}{H^2}\right]\theta_0'' - R\theta_0' + Nt\theta_0'^2 + Nb\phi_0'\theta_0' + 2Ec\Delta_1 u_0'^4 + Ecu_0'^2 + EcM^2 u_0^2 = 0, \quad \ldots (20)$$

$$\left[\left(1 + \frac{4Rd}{3}\right)\frac{1}{\Pr} - \frac{\Delta R^2}{H^2}\right]\theta_1'' - \left(1 + 2i\Delta\right) R\theta_1' + 2Nt\theta_1'\theta_0' + Nb\left(\theta_1'\phi_0' + \theta_0'\phi_1'\right) + \left(\Delta - i\right) H^2\theta_1 + 8Ec\Delta_1 u_0'^3 u_1' + 2Ecu_0' u_1' + 2EcM^2 u_0 u_1 = 0, \quad \ldots (21)$$

$$\phi_0'' - R\Pr Le\phi_0' + \frac{Nt}{Nb}\theta_0'' - \gamma_1 \Pr Le\phi_0 - K_1 \Pr Le = 0, \quad \ldots (22)$$

$$\phi_1'' - R\Pr Le\phi_1' + \frac{Nt}{Nb}\theta_1'' - \left(\gamma_1 + iH^2\right)\Pr Le\phi_1 = 0. \quad \ldots (23)$$

The appropriate B.Cs are :

$$u_0(0) = 0,\ u_1(0) = 0,\ \theta_0(0) = 0,\ \theta_1(0) = 0,\ \phi_0(0) = 0,\ \phi_1(0) = 0, \quad \ldots (24)$$

$$u_0(1) = 0,\ u_1(1) = 0,\ \theta_0(1) = 1,\ \theta_1(1) = 0, \phi_0(1) = 1,\ \phi_1(1) = 0. \quad \ldots (25)$$

Further, the dimensionless Nusselt *(Nu)* and Sherwood *(Sh)* numbers i.e., heat transfer rate and mass transfer rate respectively at the channel walls are defined as

$$Nu = \left(1 + \frac{4Rd}{3}\right)\left(\theta_0' + \varepsilon e^{it}\theta_1'\right)_{y=0,1}, \quad \ldots (26)$$

$$Sh = \left(\phi_0' + \varepsilon e^{it}\phi_1'\right)_{y=0,1}. \quad \ldots (27)$$

The shooting technique with the aid of Runge-Kutta fourth-order scheme is employed to solve the set of ODEs (18)-(23) with the B.Cs (24)-(25). The solution criteria for convergence is set to 1×10^{-10} precision and the step size is fixed with 0.001 (i.e. $\Delta y = 0.001$).

Analysis of entropy generation

Entropy generation is calculated with the aid of thermodynamics second law and is defined as

Local entropy generation rate (EG) = mass and heat transfer irreversibility + fluid friction irreversibility + Joule heating irreversibility.

$$EG = \frac{k_f}{T_1^2}\left[1 + \frac{16\sigma^* T_1^3}{3\kappa^* k_f}\right]\left(\frac{\partial T^*}{\partial y^*}\right)^2 + \frac{\sigma_f B_0^2 u^{*2}}{T_1} + \frac{\mu_f}{T_1}\left(\frac{\partial u^*}{\partial y^*}\right)^2 + \frac{2\beta_3}{T_1}\left(\frac{\partial u^*}{\partial y^*}\right)^4 + \frac{\tilde{R}D}{C_1}\left(\frac{\partial C^*}{\partial y^*}\right)^2 + \frac{\tilde{R}D}{T_1}\left(\frac{\partial C^*}{\partial y^*}\right)\left(\frac{\partial T^*}{\partial y^*}\right) \quad \ldots.(28)$$

Using the Eq. (8) in Eq. (28), the non-dimensional local entropy generation rate is

$$EG = EG_0\left[\left(1 + \frac{4Rd}{3}\right)\left(\frac{\partial\theta}{\partial y}\right)^2 + \frac{M^2 EcPr}{\delta}u^2 + \frac{Ec\Pr}{\delta}\left(\frac{\partial u}{\partial y}\right)^2 + \frac{2\Delta_1 EcPr}{\delta}\left(\frac{\partial u}{\partial y}\right)^4 + L\left(\frac{\xi}{\delta^2}\right)\left(\frac{\partial\phi}{\partial y}\right)^2 + \left(\frac{L}{\delta}\right)\left(\frac{\partial\phi}{\partial y}\right)\left(\frac{\partial\theta}{\partial y}\right)\right], \quad \ldots(29)$$

here, $EG_0 = \frac{k_f}{T_1^2}\left(\frac{T_1 - T_0}{h}\right)^2$ is characteristic entropy generation rate, $\delta = \frac{T_1 - T_0}{T_1}$ is temperature difference, $\xi = \frac{C_1 - C_0}{C_1}$ is concentration difference, $L = \frac{\tilde{R}D(C_0 - C_1)}{k_f}$ is diffusion parameter, $\tilde{R}$ is gas constant, D is diffusion term.

The entropy generation rate (NG) = $\frac{EG}{EG_0}$

$$NG = \left(1 + \frac{4Rd}{3}\right)\left(\frac{\partial\theta}{\partial y}\right)^2 + \frac{M^2 EcPr}{\delta}u^2 + \frac{EcPr}{\delta}\left(\frac{\partial u}{\partial y}\right)^2 + \frac{2\Delta_1 EcPr}{\delta}\left(\frac{\partial u}{\partial y}\right)^4 + L\left(\frac{\xi}{\delta^2}\right)\left(\frac{\partial\phi}{\partial y}\right)^2 + \left(\frac{L}{\delta}\right)\left(\frac{\partial\phi}{\partial y}\right)\left(\frac{\partial\theta}{\partial y}\right) \quad \ldots(30)$$

Bejan number (Be) = $\frac{\textit{Heat and mass transfer irreversibility}}{\textit{Entropy generation rate}}$

$$Be=\frac{\left(1+\frac{4Rd}{3}\right)\left(\frac{\partial\theta}{\partial y}\right)^2++L\left(\frac{\xi}{\delta^2}\right)\left(\frac{\partial\phi}{\partial y}\right)^2+\left(\frac{L}{\delta}\right)\left(\frac{\partial\phi}{\partial y}\right)\left(\frac{\partial\theta}{\partial y}\right)}{\left(\begin{array}{c}\left(1+\frac{4Rd}{3}\right)\left(\frac{\partial\theta}{\partial y}\right)^2+\frac{M^2EcPr}{\delta}u^2+\frac{EcPr}{\delta}\left(\frac{\partial u}{\partial y}\right)^2+\frac{2\Delta_1EcPr}{\delta}\left(\frac{\partial u}{\partial y}\right)^4\\ +L\left(\frac{\xi}{\delta^2}\right)\left(\frac{\partial\phi}{\partial y}\right)^2+\left(\frac{L}{\delta}\right)\left(\frac{\partial\phi}{\partial y}\right)\left(\frac{\partial\theta}{\partial y}\right)\end{array}\right)} \quad \ldots (31)$$

Table 1 presents the comparison between the present results and results obtained by ND Solve. Two different types of mathematical software packages namely bvp4c in MATLAB and ND Solve in Mathematica are used to validate the results of the present analysis, because there is a lack in experimental studies related to the current model. The tabulated values show that there is good agreement in between the obtained values.

Results and Discussion

In the current section, we discuss the impacts of various physical parameters such as Hartmann number (M), cross flow Reynolds number (R), non-Newtonian parameter (Δ_1), frequency parameter (H), Radiation parameter (Rd),thermal relaxation time parameter (Δ), Eckert number (Ec), thermophoresis parameter (Nt), Brownian motion parameter (Nb), material parameter (γ), chemical reaction parameter (γ_1), Lewis number (Le) on velocity, temperature, nanoparticles concentration, entropy (NG), and Bejan number (Be)through graphical representation which are shown in Figs. 2-9. The values are assigned to the parameters as follows, M =2, R = 2, Pr =21, Ec =1, H =3, Rd =2, γ = 1, Δ_1=1, λ_0 = 3, λ_1 = 2, Nb =0.2, Nt =0.3, Δ = 0.1, γ_1=1, $t=\pi/3$, Le =0.2, K_1 =0.001, L =0.01, δ =0.3, ξ =0.3, ε =0.1 unless otherwise stated. The steady velocity (u_0) profiles for various parameters M, R, and Δ_1 are rendered graphically in Figs. 2(a)-2(c). Fig. 2(a) illustrates that steady velocity is a decelerating function of Hartmann number. This is happened due to the delaying forces (Lorentz forces) create a resistive drag force which opposes the flow when the magnetic field is applied, as a resultreduction in velocity. Fig. 2(b) depicts that an increment in cross flow Reynolds number declines the velocity near the injection wall and rises the velocity near the suction wall because the inertial forces are produced by the rising values of R which causes the flow velocity fall or rise. Fig. 2(c) shows that the velocity diminished for the higher values of Δ_1. This is due to the fact that augmenting Δ_1 magnifies the viscoelasticity which reduces the velocity.

Figures 3(a-f) portrayed the unsteady velocity (u_t) profiles of M, R, H, γ, Δ_1, and t. Figure 3(a) depicts that u_t is a decreasing function of Hartmann

Table 1 — Comparison of present results with ND Solve for Nu and Sh at $y=0$ when R=0.3, H= 3, M = 2, Δ_1 = 1, Pr =21, Ec = 1, Nb = 0.2, Nt = 0.3, Rd = 1, $t=\pi/3$, λ_0 = 3, λ_1 = 2, γ =1, γ_1 =1, Le =0.2, K_1 =0.001, Δ = 0.1, and ε = 0.1

Parameters	Values	Present results		ND Solve	
		Nu	*Sh*	*Nu*	*Sh*
Ec	0.1	4.59527066	-0.71006252	4.59531712	-0.71008974
	0.3	5.64788585	-1.23276389	5.64788603	-1.23276400
	0.6	7.33753543	-2.07865740	7.33754189	-2.07866124
M	0	10.34368124	-3.68250145	10.34371787	-3.68252313
	2	9.82813677	-3.33974915	9.82813680	-3.33974917
	4	8.18937927	-2.42659532	8.18937935	-2.42659537
Δ_1	1	9.82813677	-3.33974915	9.82813680	-3.33974917
	2	9.00734623	-2.92660846	9.00735114	-2.92661138
	3	8.53977035	-2.69184876	8.54038510	-2.69221489
Nt	0.2	7.02190115	-1.15348092	7.02192132	-1.15348881
	0.4	13.75977250	-7.46108549	13.75980496	-7.46111151
	0.6	24.77313563	-24.29335481	24.77548083	-24.29623784

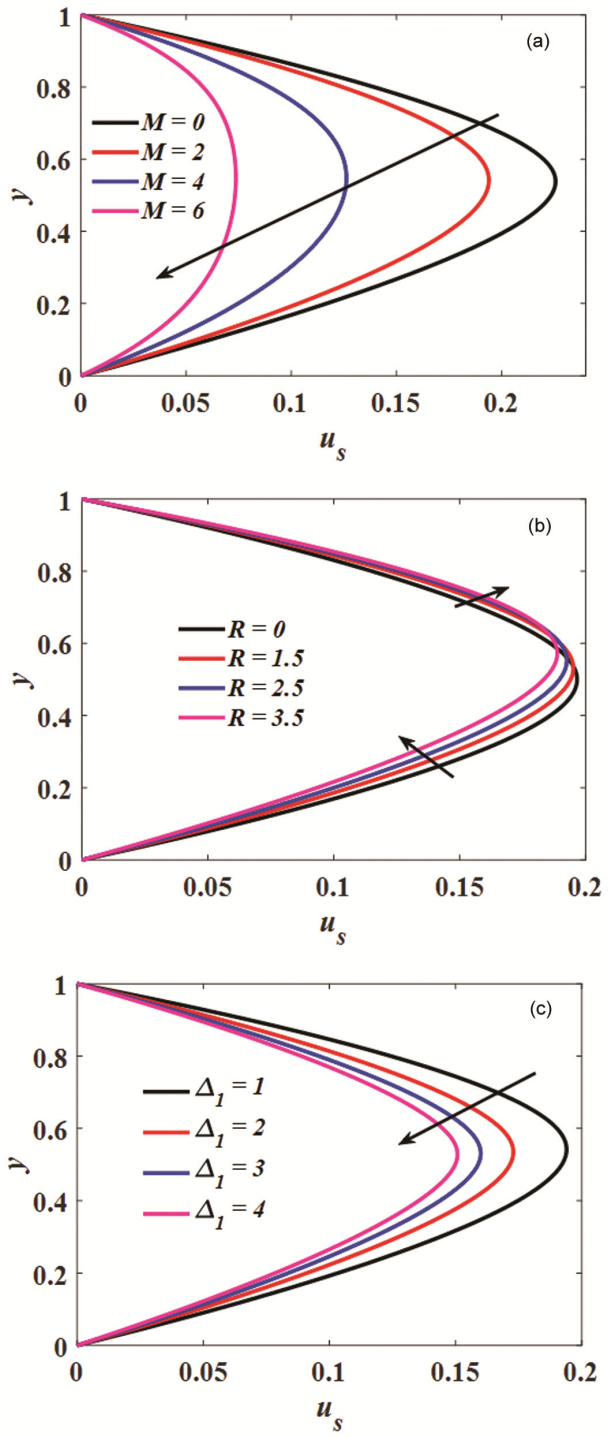

Fig. 2 — Steady velocity profiles (a) Effect of *M*; (b) Effect of R and (c) Effect of Δ_1.

number. This is because of retarding forces which acts as a resistive drag force and slows down the flow velocity. Fig. 3(b) displays that intensifying R declines the velocity near the injection wall and accelerates the velocity near the suction wall. A rise in H diminishes the unsteady velocity of nanofluid because the amplitude of oscillations increases for the higher values of H (see Fig. 3(c)). The unsteady velocity is a declining function of γ and Δ_1 because magnifying the values of γ and Δ_1 magnifies the viscoelasticity of the nanofluid which causes reduction in u_t (see Figs 3(d-e)). Figure 3(f) depicts that for various t values there exists an oscillating behaviour in u_t.

Figures 4(a-i) are plotted to elucidate the effects of Ec, R, M, Nt, Nb, H, Rd, Δ_1, and Δ on the steady temperature (θ_s) of third-grade nanoliquid. A rise in viscous dissipation upsurges the temperature due to the frictional heating between channel walls and fluid molecules (see Fig. 4(a)). Figure 4(b) elucidates that intensifying cross flow Reynolds number reduces θ_s because a rise in R slows down the energy transportation from channel walls, due to this reason reduction happens in θ_s. The similar trend can be found for the higher values of Hartmann number in Fig. 4(c). Since the velocity is decreased due to the Lorentz forces for rising values of M leads to weakening the thermal energy transportation caused by the advection phenomena. The influence of thermophoresis and Brownian motion parameters on θ_s are displayed in Figs 4(d-e). From these figures, one can notice that augmenting Nt and Nb accelerates the steady temperature because boosting the values of Nt and Nb helps the thermal energy particles to spread the energy from high-level to low-level temperature by the random motion of the nanoparticles.Figure 4(f) illustrates that magnifying the values of H escalates the temperature of the nanoliquid. A similar behaviour is observed for uplifting the radiation parameter because for the higher values of Rd supports to produce the additional energy in the fluid region (see Fig. 4(g)). Figure 4(h) displays that θ_s is a decreasing function of non-Newtonian parameter because an enhancement in Δ_1 accelerates the visco-elasticity of the nanofluid. The same characteristic can be found for the augmenting values of thermal relaxation time parameter which is portrayed in Fig. 4(i). This is happened because the higher thermal relaxation time requires additional

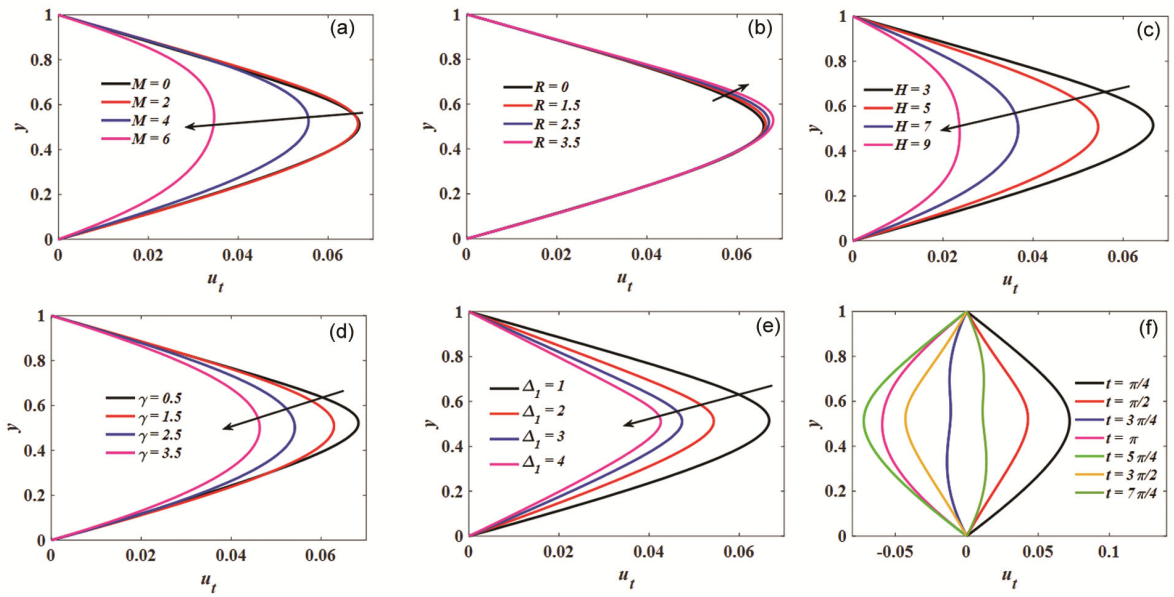

Fig. 3 — Unsteady velocity profiles (a) Effect of *M*; (b) Effect of *R*; (c) Effect of *H*; (d) Effect of γ ; (e) Effect of Δ_1 and (f) Effect of t .

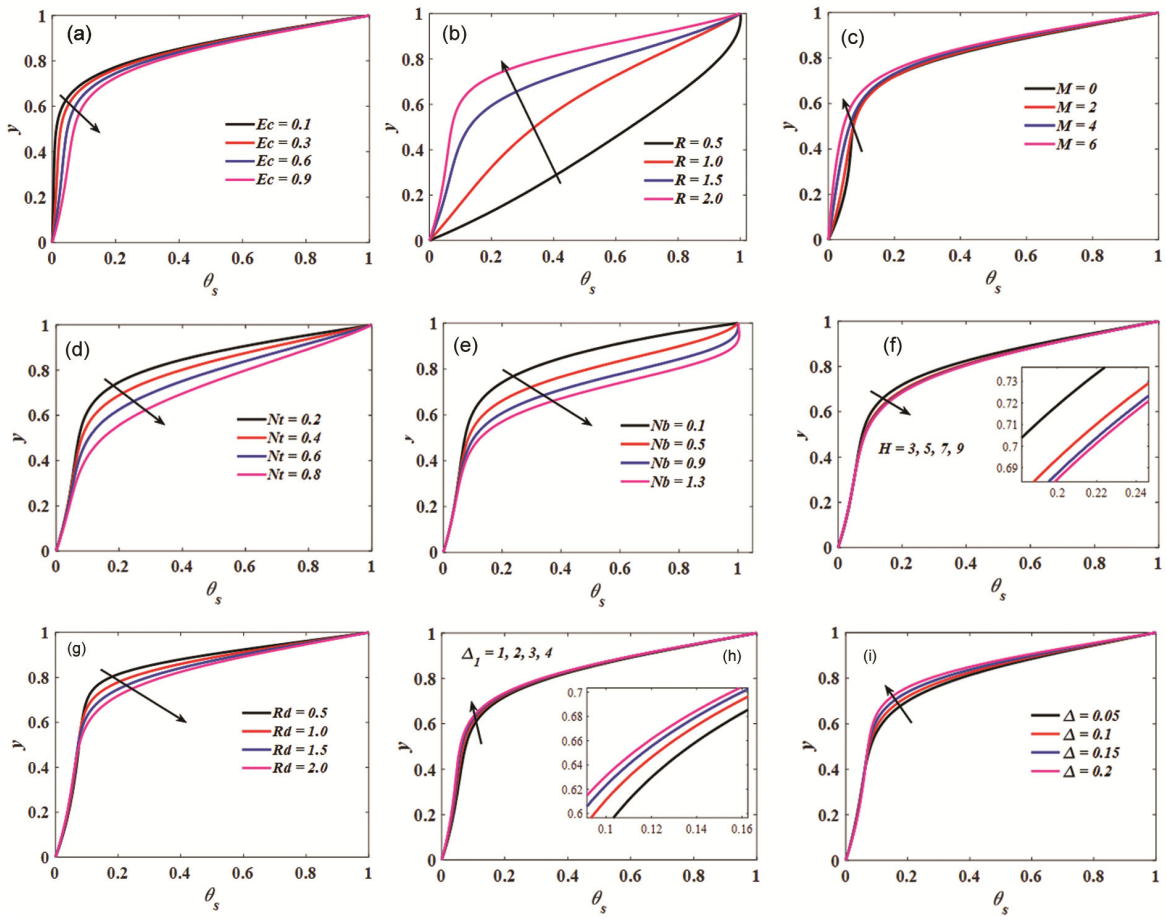

Fig. 4 — Steady temperature profiles (a) Effect of *Ec*; (b) Effect of *R*; (c) Effect of *M*; (d) Effect of *Nt*; (e) Effect of *Nb*; (f) Effect of *H*; (g) Effect of *Rd*; (h) Effect of Δ_1 and (i) Effect of Δ .

time for thermal conduction to neighbouring nanoparticles.

The impressions of various parameters like Ec, R, M, Nt, Nb, H, Rd, Δ_1, Δ, and t on the unsteady temperature (θ_t) of third-grade nanoliquid are depicted graphically in Figs. 5(a-j). Figure 5(a) shows the effect of Eckert number on unsteady temperature profiles. From this figure, one can infer that intensifying Ec enhances the temperature towards the bottom wall and shows an oscillating nature in θ_t. An increment in cross flow Reynolds number displays a wavering behaviour in θ_t (see Fig. 5(b)). Figure 5(c) deliberated that there is an oscillating trend in θ_t for the augmenting values of M. The similar kind of behaviour exists in θ_t for the higher values of Nt and Nb due to the random motion of nanoparticles in fluid domain

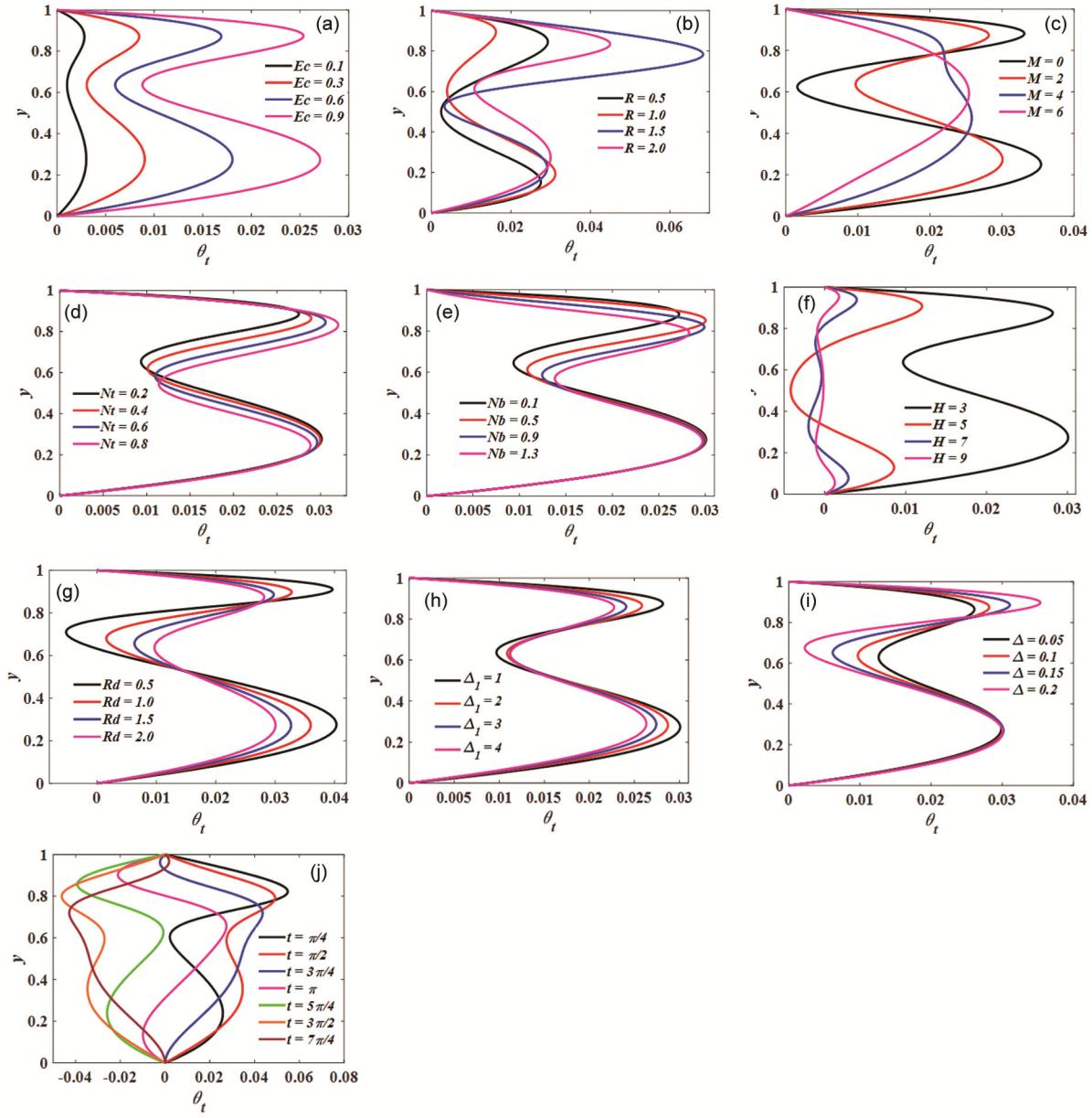

Fig. 5 — Unsteady temperature profiles (a) Effect of *Ec*; (b) Effect of *R*; (c) Effect of *M*; (d) Effect of *Nt*; (e) Effect of *Nb*; (f) Effect of *H*; (g) Effect of *Rd*; (h) Effect of Δ_1, (i) Effect of Δ and (j) Effect of t.

(see Figs. 5(d) and 5(e)). Figure 5(f) presents that there is a wavering nature in θ_t for escalating values of H. Augmenting the radiation parameter displays an oscillating character in unsteady temperature profiles (see Fig. 5(g)). The similar nature can be found in θ_t for an enhancement in non-Newtonian parameter and thermal relaxation time parameter (see Figs. 5(h) and 5(i)). Figure 5(j) reveals that there is an oscillating nature in θ_t for various values of t and the maximum temperature is near the upper wall of the channel.

The influence of radiation parameter, chemical reaction parameter, Lewis number, Brownian motion parameter, and thermophoresis parameter on steady concentration of nanoparticles (ϕ_s) are deliberated in Figs. 6(a-e). Figure 6(a) shows that an enhancement

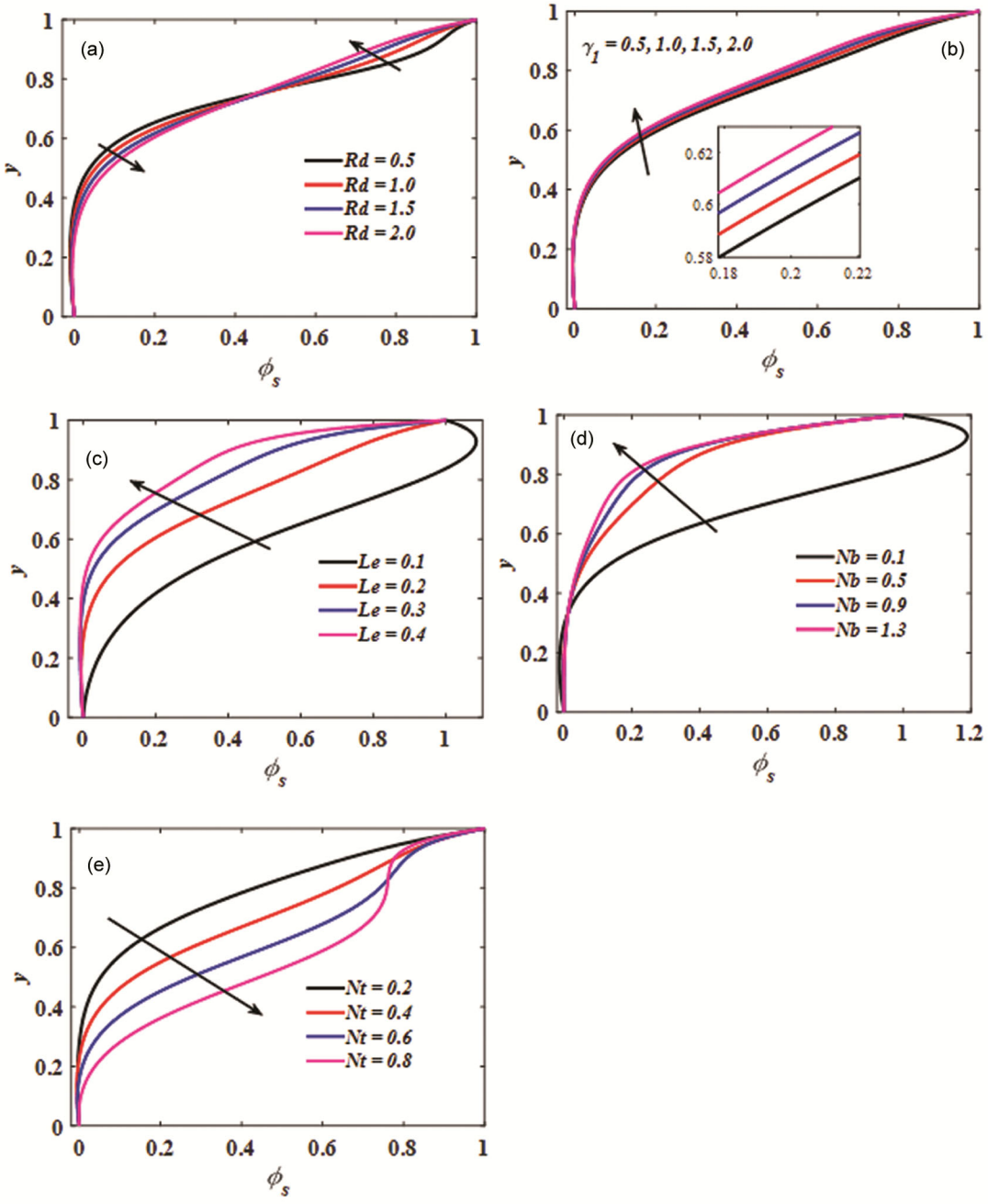

Fig. 6 — Steady concentration profiles (a) Effect of *Rd*; (b) Effect of γ_1; (c) Effect of *Le*; (d) Effect of *Nb* and (e) Effect of *Nt*.

in Rd enhances the concentration of nanoparticles near the injection wall and reduces ϕ_s near the suction wall. ϕ_s decelerates for the magnifying values of chemical reaction parameter (see Fig. 6(b)). Figure 6(c) illustrates that a rise in Le reduces the concentration of nanoparticles because increasing Le intensifies the mass transfer rate which causes the reduction in ϕ_s. Accelerating the values of Brownian motion parameter declines ϕ_s, whereas for augmenting values of Nt enhances the steady concentration due to the random movement of particles (see Figs. 6(d) and 6(e)). Figures 7(a-e) portrayed the impact of Rd, γ_1, Le, Nb, and Nt on unsteady concentration of nanoparticles (ϕ_t). Figure 7(a) presents that for rising values of Rd there is an oscillating trend in ϕ_t. A similar kind of character can be noticed in ϕ_t for enhancing the chemical reaction parameter (see Fig. 7(b)). Figure 7(c) reveals that ϕ_t shows the wavering nature for the higher values of Lewis number. Figures 7 (d) and 7(e) elucidate that intensifying the values of Nb and Nt cause an oscillating behaviour in ϕ_t due to the random motion of nanoparticles.

Figures 8(a-d) are plotted to display the impact of radiation parameter, Hartmann number, Eckert number, and temperature difference on entropy generation rate (*NG*). Figure 8(a) depicts that a rise in Rd rises NG because the thermal conductivity of the nanoliquid enhanced for the higher values of Rd. It is noticed that uplifting the values of M shows an oscillating nature in *NG* due to the Lorentz forces (see Fig. 8(b)). Further, from the same figure, one can infer that the higher magnetic field slows down the entropy near the channel walls. Figure 8(c) illustrates that accelerating Ec upsurges the entropy generation rate because intensifying Ec produces more energy due to the frictional heating. The opposite nature can be noticed for increasing values of δ in *NG* (see Fig. 8(d)).

The effects of Rd, M, Ec, and δ on Bejan number (Be) are deliberated in Figs. 9(a-d). Figure 9(a) elucidates the impression of radiation parameter on Be. From the same figure, one can observe that increasing Rd enhances the Bejan number because improving Rd improves the thermal efficiency of the fluid. The similar kind of nature can be noticed in Be for the rising values of M (see Fig. 9(b)). Figure 9(c) displays that intensifying the Eckert number decelerates the Bejan number due to the frictional heating. The reverse

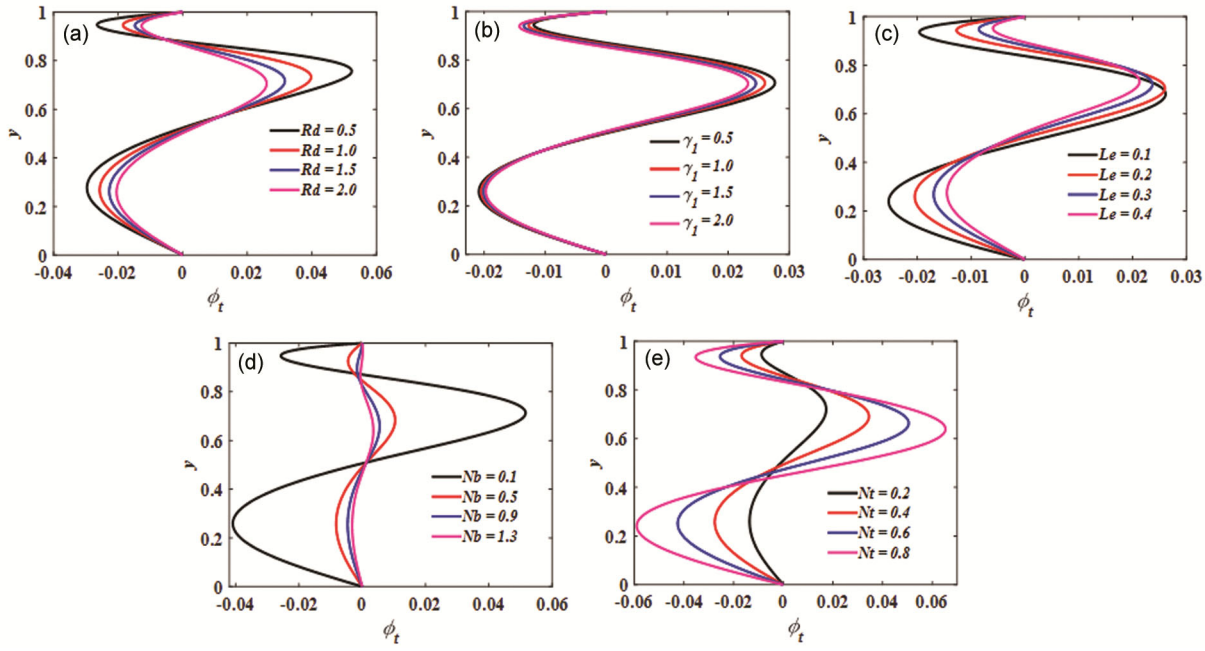

Fig. 7— Unsteady concentration profiles (a) Effect of *Rd*; (b) Effect of γ_1; (c) Effect of *Le*; (d) Effect of *Nb* and (e) Effect of *Nt*.

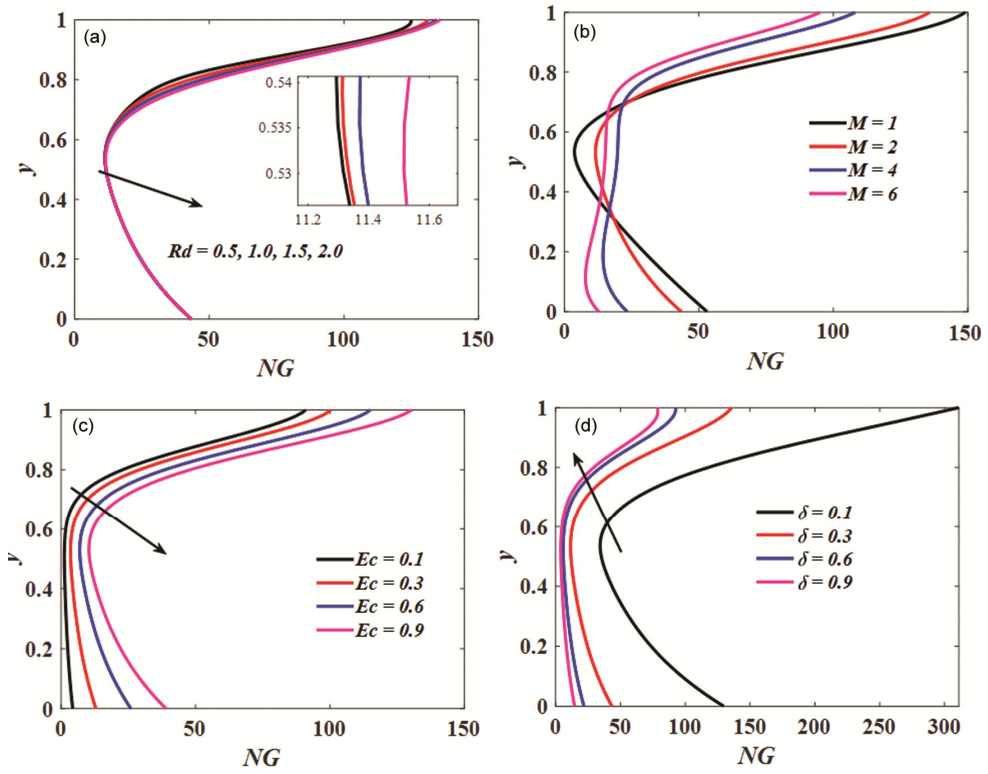

Fig. 8 — Entropy distribution profiles (a) Effect of *Rd*; (b) Effect of *M*; (c) Effect of *Ec* and (d) Effect of δ.

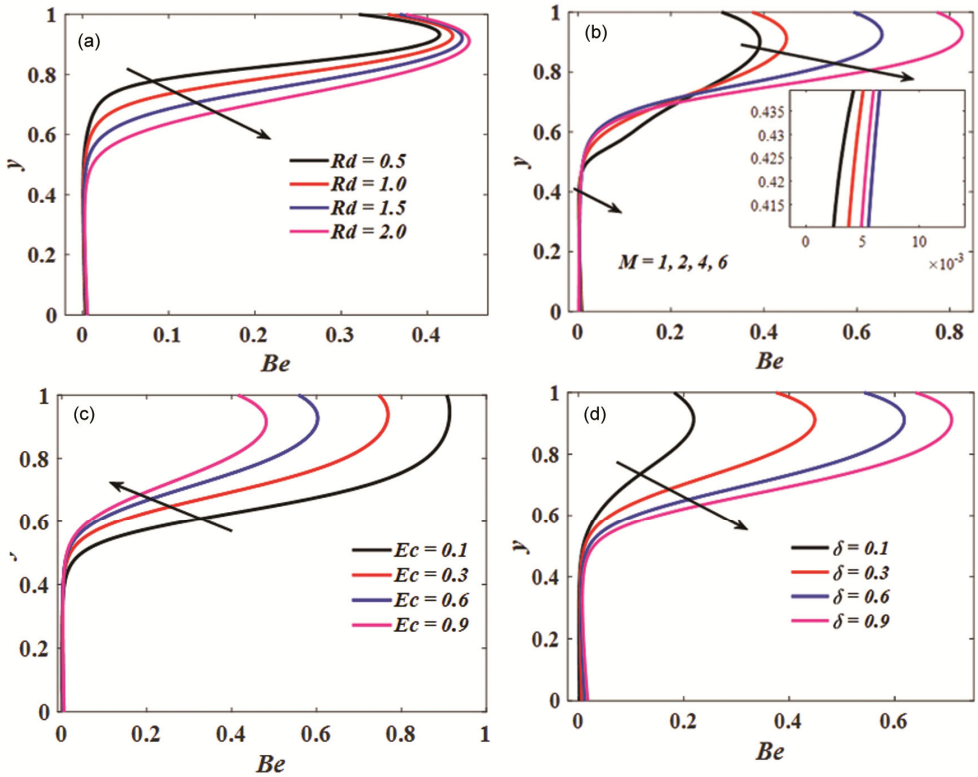

Fig. 9 — Bejan number distribution profiles (a) Effect of *Rd*; (b) Effect of *M*; (c) Effect of *Ec* and (d) Effect of δ.

Table 2 — Variations in heat and mass transfer rates at $y = 0$ for various physical parameters when R=2, H= 3, $M = 2$, $\Delta_1 = 1$, Pr =21, $Ec = 1$, $Nb = 0.2$, $Nt = 0.3$, $Rd = 1$, Δ =0.1, $t = \pi/3$, $\lambda_0 = 3$, $\lambda_1 = 2$, γ =1, γ_1 =1, Le =0.2, K_1 =0.001, and $\varepsilon = 0.1$

Parameters	Values	At bottom wall $y = 0$	
		Nu	*Sh*
	0	0.90579490	-0.15221330
M	2	0.67832020	-0.10293651
	4	0.34632061	-0.03624822
	1	0.67832020	-0.10293651
Δ_1	2	0.62263825	-0.09565609
	3	0.58670676	-0.09072992
	0.1	0.06618771	-0.00331988
Ec	0.3	0.19962542	-0.02478231
	0.6	0.40250874	-0.05768286
	0.2	0.67832020	-0.10293651
Nb	0.4	0.67872954	-0.04921841
	0.6	0.67920011	-0.03108520
	0.1	0.66559050	-0.03352098
Nt	0.3	0.67832020	-0.10293651
	0.5	0.69261497	-0.16942251
	0.5	0.50825623	-0.11056120
Rd	1.0	0.67832020	-0.10293651
	1.5	0.83362225	-0.09478736

trend is observed in Be for the augmenting values of δ (see Fig. 9(d)).

The heat and mass transfer rates (Nu and Sh) for various pertinent parameters such as M, Δ_1, Ec, Nb, Nt, and Rd at bottom wall is given in Table 2. The distribution shows that intensifying the values of viscous dissipation, Brownian motion parameter, thermophoresis parameter, and radiation parameter intensifies the heat transfer rate whereas Nu dwindles for enhancing the values of Hartmann number and non-Newtonian parameter. In the same sense, the mass transfer rate accelerates for the magnifying values of M, Δ_1, Nb, and Rd while it decelerates for the higher values of Ec and Nt.

Conclusion

In this paper, heat and mass transfer of oscillatory hydromagnetic third grade nanofluid flow between two horizontal parallel porous walls with Cattaneo-Christov heat flux model and entropy generation analysis have been investigated. The influence of Brownian motion, thermophoresis, Ohmic heating, radiative heat have been considered. Buongiorno nanofluid model is utilized for the present analysis. These kinds of inspections are applicable in biomedical engineering, manufacturing industries as coolants, energy conservation, dynamics of physiological fluids, biomedicines, and nano-drug suspension in pharmaceuticals. The system of ODEs have been obtained and solved by utilizing shooting method with the aid of Runge-Kutta 4th order approach after the implementation of the perturbation technique on non- dimensional PDEs. Graphs have been plotted to show the effects of various nondimensional parameters in detail. The key outcomes of the present inspection are summarized as follows:

- The velocity of third-grade nanofluid declines for the magnifying values of Hartmann number, material parameter, frequency parameter, and non-Newtonian parameter.
- Accelerating thermal relaxation time parameter, Hartman number, cross flow Reynolds number reduces the temperature.
- The temperature magnifies for an increment in *H*, Ec, Rd, Nb, and Nt.
- The concentration of nanoparticles decelerates for the higher values of Le, R, γ_1, Nb while it enhances for magnifying values of Nt.
- The unsteady temperature and concentration profiles show the oscillating behaviour.
- An improvement in Rd and Ec improves the entropy production while a rise in M reduces NG.
- Accelerating Rd and M accelerates the Bejan number whereas augmenting Ec declines Be.
- The heat and mass transfer rates are accelerated for the higher values of Brownian motion parameter.

References

1 Radhakrishnamacharya G & Maiti M K, *Int J Heat Mass Transf*, 20 (1977) 171.

2 Bestman A R, *Int J Heat Mass Transf*, 25 (1982) 675.

3 Wang C Y, *J Appl Mech Trans ASME*, 38 (1971) 553.

4 Malathy T & Srinivas S, *Int Commun Heat Mass Transf*, 35 (2008) 681.

5 Shawky H M, *Heat Mass Transf*, 45 (2009) 1261.

6 Rajamani S, Reddy A S, Srinivas S & Ramamohan T R, *Indian J Pure Appl Phys*, 60 (2022) 355.

7 van Buren S, Miranda A C & Polifke W, *Int J Heat Mass Transf*, 144 (2019) 118585.
8 Zhang F, Bian Y, Liu Y, Pan J, Yang Y & Arima H, *Int J Heat Mass Transf*, 141 (2019) 1168.
9 Kardgar A, *Eur Phys J Plus*, 136 (2021) 1.
10 Govindarajulu K & Subramanyam Reddy A, *Phys Fluids*, 34 (2022) 013105.
11 El Kot M A & Abd Elmaboud Y, *J Therm Anal Calorim*, 147 (2022) 4355.
12 Hatami M, Hatami J & Ganji D D, *Comput Methods Programs Biomed*, 113 (2014) 632.
13 Sinha A, *Alexandria Eng J*, 54 (2015) 1243.
14 Venkatesan G & Reddy A S, *Indian J Pure Appl Phys*, 60 (2022) 437.
15 Wang L, Jian Y, Liu Q, Li F & Chang L, *Colloids Surfaces A Physicochem Eng Asp*, 494 (2016) 87.
16 Abou-zeid M Y & Ouaf M E, *Case Stud Therm Eng*, 28 (2021) 101362.
17 Islam S, Khan A, Deebani W, Bonyah E, Alreshidi N A & Shah Z, *AIP Adv*, 10 (2020) 055015.
18 Ijaz Khan M, Nigar M, Hayat T & Alsaedi A, *Comput Methods Programs Biomed*, 187 (2020) 105221.
19 Waqas H, Wakif A, Al-Mdallal Q, Zaydan M, Farooq U & Hussain M, *Alexandria Eng J*, 61 (2022) 1425.
20 Choi S U S & Eastman J A, *Am Soc Mech Eng Fluids Eng Div FED*, 231 (1995) 99.
21 Souza R R, Gonacalves M I, Rodrigues O R, Minas G, Miranda J M, Moreira L N A,Lima R, Coutinho G, Pereira J E & Moita S A, *Appl Therm Eng*, 201 (2022) 117725.
22 Nandhini G & Shobana M K, *J Magn Magn Mater*, 552 (2022) 169236.
23 Govindarajulu K & Subramanyam Reddy A, *J Process Mech Eng*, 236 (2022) 1544.
24 Chaudhary S, *Indian J Chem Technol*, 29 (2022) 311.
25 Buongiorno J, *J Heat Transfer*, 128 (2006) 240.
26 Shah Z, Gul T, Islam S, Khan M A, Bonyah E, Hussain F, Mukhtar S & Ullah M, *Results Phys*,10 (2018) 36.
27 Chu Y M, Khan M I, Khan B N, Kadry S & Khan S U, *Int Commun Heat Mass Transf*, 118 (2020) 104893.
28 Bejan A, *J Heat Transfer*, 101 (1979) 718.
29 Loganathan K, Mohana K, Mohanraj M, Sakthivel P & Rajan S, *J Therm Anal Calorim*, 144 (2021) 1935.
30 Li Y X, Khan M I, Gowda R J P, Ali A, Farooq S, Chu Y M & Khan S U,*Chinese J Phys*, 73 (2021) 275.
31 Sultan F, Khan W A, Ali M, Shahzad M, Sun H & Irfan M, *J Brazilian Soc Mech Sci Eng*, 41 (2019) 1.
32 Ijaz Khan M, Hafeez M U, Hayat T, Imran Khan M & Alsaedi A, *Comput Methods Programs Biomed*, 183 (2020) 105093.
33 Dogonchi A S & Ganji D D, *J Taiwan Inst Chem Eng*, 80 (2017) 52.
34 Doh D H, Cho G R, Ramya E & Muthtamilselvan M, *Case Stud Therm Eng*, 14 (2019) 1.
35 Cattaneo C, *Atti Sem Mat Fis Univ Modena*, 3 (1948) 83.
36 Christov C I, *Mech Res Commun*, 36 (2009) 481.
37 Hayat T, Khan S A, Ijaz Khan M, Momani S & Alsaedi A, *Comput Methods Programs Biomed*, 187 (2020) 105247.
38 Khan S A, Hayat T & Alsaedi A, *Chinese J Phys*, 76 (2022) 205.
39 Ahmad S, Nadeem S, Muhammad N & Khan M N, *J Therm Anal Calorim*, 143 (2021)1187.